Scientific Research Publishing

Open Journal of Applied Sciences, 2017, 7, 520-536
http://www.scirp.org/journal/ojapps
ISSN Online: 2165-3925
ISSN Print: 2165-3917

Modeling and Characterization of Vegetation, Aquatic and Mineral Surfaces Using the Theory of Plausible and Paradoxical Reasoning from Satellite Images: Case of the Toumodi-Yamoussoukro-Tiébissou Zone in V Baoulé (Côte d'Ivoire)

Jean-Claude Okaingni[1,2], Sié Ouattara[1,2], Adles Kouassi[1,2,3], Wognin J. Vangah[1,2], Aubin K. Koffi[1,2], Alain Clement[4]

[1]Laboratory of Signals and Electrical Systems (L2SE), Institut National Polytechnique Houphouët Boigny, Yamoussoukro, Cote D'Ivoire
[2]Institut National Polytechnique Houphouët Boigny (INPHB), Yamoussoukro, Cote D'Ivoire
[3]Ecole Supérieure des Technologies de l'Information et de la Communication (ESATIC), Abidjan, Cote D'Ivoire
[4]Institut Universitaire de Technologie d'Angers (IUT), Angers, France
Email: sie_ouat@yahoo.fr

How to cite this paper: Okaingni, J.-C., Ouattara, S., Kouassi, A., Vangah, W.J., Koffi, A.K. and Clement, A. (2017) Modeling and Characterization of Vegetation, Aquatic and Mineral Surfaces Using the Theory of Plausible and Paradoxical Reasoning from Satellite Images : Case of the Toumodi-Yamoussoukro-Tiébissou Zone in V Baoulé (Côte d'Ivoire). *Open Journal of Applied Sciences*, **7**, 520-536.
https://doi.org/10.4236/ojapps.2017.710038

Received: September 21, 2017
Accepted: October 23, 2017
Published: October 26, 2017

Abstract

In this paper, the theory of plausible and paradoxical reasoning of Dezert-Smarandache (DSmT) is used to take into account the paradoxical character through the intersections of vegetation, aquatic and mineral surfaces. In order to do this, we developed a classification model of pixels by aggregating information using the DSmT theory based on the PCR5 rule using the *NDVI*, *MNDWI* and *NDBaI* spectral indices obtained from the ASTER satellite images. On the qualitative level, the model produced three simple classes for certain knowledge (E, V, M) and eight composite classes including two union classes characterizing partial ignorance ({E,V}, {M,V}) and six classes of intersection of which three classes of simple intersection (E∩V, M∩V, E∩M) and three classes of composite intersection (E∩{M,V}, M∩{E,V}, V∩{E,M}), which represent paradoxes. This model was validated with an average rate of 93.34% for the well-classified pixels and a compliance rate of the entities in the field of 96.37%. Thus, the model 1 retained provides 84.98% for the simple classes against 15.02% for the composite classes.

Keywords

Theory of Plausible and Paradoxical Reasoning, PCR5 Rule, ASTER Satellite

Images, *NDVI*, *MNDWI*, *NDBaI,* Modeling, Classification

1. Introduction

The surface state of the Earth can be represented in remote sensing by three entities that are vegetation surfaces, aquatic surfaces and mineral surfaces. Any surface area observed, depending on the size of the area, may be a combination of these three entities.

Thus, it can be observed vegetation surface, aquatic surface, mineral surface, vegetation and aquatic surface, vegetation and mineral surface, mineral and aquatic surface, vegetation, mineral and aquatic surface.

The use of satellite images, for mapping purposes, has been the subject of several studies ([1] [2] [3] [4]). Researchers have used spectral indices to map vegetation surfaces, aquatic surfaces, and surfaces of bare soil and mansions.

These indices were used for image classification. Unfortunately, imperfections (uncertainties, inaccuracies, etc.) on the information produced by the images associated with said indices are observed ([5] [6]). Taking into account and good management of these imperfections are done by the theory of belief functions.

The Dempster-Shafer theory has been used successfully to handle cases of uncertainty, vagueness and ignorance in the classification of pixels to classes of vegetation surface, aquatic surface and mineral surface [4].

In this article, the theory of plausible and paradoxical reasoning of Dezert-Smarandache (DSmT) is used to take into account the paradoxical character through the intersections of the elements vegetation surface, aquatic surface and mineral surface.

The general objective of the study is to develop a model of pixel classification by aggregating information using the DSmT theory, spectral indices *NDVI* (Normalized Difference Vegetation Index), *MNDWI* (Modification of Normalized Difference Water Index) and *NDBaI* (Normalized Difference Bare Index) and ASTER satellite images. It acts specifically first, to model the frameworks of discernment and reasoning and belief functions, then define the decision criteria and write algorithms and programming codes under the MATLAB software; finally realize and evaluate classified image.

The contribution of this study is to give an approach of unsupervised classification of mapping that takes into account the plausible and paradoxical characteristics related to the information of ground that is to say without needing to know the real spatial state of the ground concerned.

This paper, which proposes to report on the work carried out, presents successively the theory of plausible and paradoxical reasoning of Dézert-Smarandache, the material used, the methodological approach that guided the work and the results obtained.

2. Principle and Formalism of DSmT

Dezert-Smarandache theory (DSmT) is interpreted as a generalization of the theory of Dempster-Shafer (DST) ([7]). Its basic principle and formalism for aggregating information can be characterized by a four-stage structure of modeling, estimation, combination and decision.

Modeling consists in choosing the representation of the frameworks of discernment and reasoning and the models of the mass functions to be used.

The discernment framework $\Theta = \{\theta_1, \cdots, \theta_N\}$ of DSmT is an exhaustive set of different hypotheses, not necessarily exclusive assumptions. The reasoning framework D^Θ associated, also called hyper-powerset, is the set of all possible propositions constructed from the elements of Θ, including the empty set (ϕ), with the operators $\cup$ and $\cap$. It is characterized by the following conditions ([8]):

1) $\phi, \theta_1, \cdots, \theta_N \in D^\Theta$,

2) If $A_i, A_j \in D^\Theta$ then $A_i \cap A_j \in D^\Theta$ and $A_i \bigcup A_j \in D^\Theta$,

3) There are no other elements belonging to D^Θ, except those obtained using rules 1 or 2.

The construction of the reasoning framework D^Θ can be obtained by a matrix product between the binary matrix of Dedekind and the coding vector of Smarandache ([1] [7]). Its cardinal increases according to the cardinal of the discernment framework on which it is based.

In order to fix ideas, it is considered the cardinal of Θ equal to 3. Thus, according to Dedekind ([9]), the cardinal of D^Θ is equal to 19. Then we get ([1]):

$$\Theta = \{\theta_1, \theta_2, \theta_3\}$$

$$\begin{aligned} D^\Theta = \{&\phi, \theta_1, \theta_2, \theta_3, \theta_1 \cup \theta_2, \theta_2 \cup \theta_3, \theta_1 \cup \theta_3, \theta_1 \cup \theta_2 \cup \theta_3, \theta_1 \cap \theta_2, \\ &\theta_2 \cap \theta_3, \theta_1 \cap \theta_3, \theta_1 \cap (\theta_2 \cup \theta_3), \theta_3 \cap (\theta_1 \cup \theta_2), \theta_2 \cap (\theta_1 \cup \theta_3), \\ &\theta_2 \cup (\theta_1 \cap \theta_3), \theta_3 \cup (\theta_1 \cap \theta_2), \theta_1 \cup (\theta_2 \cap \theta_3), \\ &(\theta_1 \cap \theta_3) \cup (\theta_1 \cap \theta_2) \cup (\theta_2 \cap \theta_3), \theta_1 \cap \theta_2 \cap \theta_3\} \end{aligned}$$

In general, we define a generalized mass function m of D^Θ with values in [0,1] satisfying the following conditions of Equation (1):

$$\begin{cases} \sum_{A \in D^\Theta} m(A) = 1 \\ m(\phi) = 0 \end{cases} \tag{1}$$

where ϕ is the empty set. The value $m(A)$ quantifies the belief that the class sought belongs to the subset A of D^Θ (and to no other subset of A). The subsets A such that $m(A) > 0$ are called focal elements.

The following special mass functions are defined ([10]):

- ✓ a mass function m is said to be **normal** when $m(\phi) = 0$;
- ✓ a mass function m is said to be **categorical** when it has a single focal element A such that $m(A) = 1$. In the case where A is a set, knowledge is certain but imprecise.

When $A = \{\theta_k\}$, knowledge is certain and precise;

- ✓ a mass function m is said to be **empty** (or **total ignorance**) when the function m is categorical in Θ: $m(\Theta) = 1$;
- ✓ a mass function m is said to be **Bayesian** if all the focal elements are singletons of Θ in Equation (2):

$$\sum_{\theta_k \in \Theta} m(\theta_k) = 1; \tag{2}$$

- ✓ a mass function m is said to be **dogmatic** if $m(\Theta) = 0$;
- ✓ a mass function m is said to be **consonant** if all the focal elements are nested;
- ✓ a mass function m is said to have a **simple support** when it has 2 focal elements, one of which is Θ (Equation (3)):

$$\begin{cases} m(A) = 1-\omega, & A \in D^{\theta} \\ m(\Theta) = \omega \\ m(B) = 0, & \forall B \in D^{\theta} \setminus A \end{cases} \tag{3}$$

In this case, the function m can also be denoted A^{ω} where ω represents the weight of the ignorance of the mass function m.

The estimation consists in determining all the parameters of the mass functions selected at the modeling stage. This is a difficult problem that does not have a universal solution. The difficulty is further increased if we want to assign masses to compound hypotheses involving intersections and/or unions ([11]).

The combination is the grouping phase of the information, from the mass functions of the different information sources, using an operator adapted to the formalism of the modeling. The DSmT has two types of combination ([12]): the classic version and the hybrid version. Consider n initial mass functions $m_1, m_2, \cdots, m_n$ representing the respective information of n different sources, which can be combined according to the DSmT.

The classic combination of DSmT is (Equation (4)):

$$\begin{gathered} m(C) = \sum_{A_1 \cap A_2 \cap \cdots \cap A_n = C} m_1(A_1) * m_2(A_2) * \cdots * m_n(A_n) \\ A_i (i = 1, \cdots, n) \in D^{\theta}, \forall C \in D^{\theta} \end{gathered} \tag{4}$$

The hybrid combination of DSmT is used in the presence of integrity constraints applied to D^{Θ}. An integrity constraint of a set U is an impossibility of considering a mass assignment to this set ([12]). The mass of the set U is then assigned to the empty set ϕ. Thus, the hybrid combination is defined ([13]) by Equations (5)-(8):

$$m(A) = \phi(A) * \left[H_1(A) + H_2(A) + H_3(A) \right], \quad \forall A \in D^{\theta} \tag{5}$$

$$H_1(A) = \sum_{\substack{X_i (i=1,\cdots,n) \in D^{\theta} \\ X_1 \cap X_2 \cap \cdots \cap Xn = A}} m_1(X_1) * m_2(X_2) * \cdots * m_n(X_n) \tag{6}$$

$$H_2(A) = \sum_{\substack{X_i (i=1,\cdots,n) \in \phi \\ \left[\bigcup_{i=1}^{n} u(X_i) = A \right] \vee \left[\left(\bigcup_{i=1}^{n} u(X_i) \in \phi \right) \wedge (A = \Theta) \right]}} m_1(X_1) * m_2(X_2) * \cdots * m_n(X_n) \tag{7}$$

$$H_3(A) = \sum_{\substack{X_i(i=1,\cdots,n)\in D^\theta \\ X_1\cup X_2\cup\cdots\cup X_n=A \\ X_1\cap X_2\cap\cdots\cap X_n=\phi}} m_1(X_1) * m_2(X_2) * \cdots * m_n(X_n) \tag{8}$$

The function $\phi(A)$ of Equation (5) is a binary function equal to zero for empty or impossible sets A and is worth the unit for the others. In Equation (7), the set $u(X_i)$ represents the union of all the objects of the set X_i. Thus, this equation indicates that if the union of objects is also a constraint, then the mass is either assigned to the union of all the singletons that form the objects, or to total ignorance. Equation (8) indicates that the mass is attributed to the union of all the objects of the sets X_i, if the intersection is a constraint.

Several rules exist to achieve a hybrid combination. The 5th version of the family of rules of combination with Proportional Redistribution of Conflict (PCR5) is presented in the following, because it gives better results ([14]).

In a simplifying process, Djiknavorian ([12]) proposes a dynamic procedure which can be put in the form of the following algorithm (Dj):

Beginning

$s_1 = m_1$

For $i = 1$ to $n-1$ do

$$s_{i+1}(C) = \sum_{\substack{A,B\in D^\theta \\ A\cap B=C}} s_i(A) * m_{i+1}(B) + \sum_{\substack{D\in D^\theta \\ D\cap C=\Phi}} \left[\frac{(s_i(C))^2 * m_{i+1}(D)}{s_i(C) + m_{i+1}(D)} + \frac{(m_{i+1}(C))^2 * s_i(D)}{m_{i+1}(C) + s_i(D)} \right], \forall C \in D^\theta$$

End

$m(C) = s_n(C), \quad \forall C \in D^\theta$

End

where m_i (i = 1 to n) represent n mass functions corresponding to n different information sources and m the combined mass function obtained by the PCR5 rule.

The most commonly used decision rules for DSmT are based on combined mass functions, credibility functions, plausibility functions or pignistic probability functions.

The functions of credibility (*Bel*), of plausibility (*Pls*) and of pignistic probability (*BetP)* are defined from D^Θ in $[0,1]$ and are given respectively by Equations (9)-(12):

$$Bel(A) = \sum_{B\in D^\theta, B\subseteq A} m(B), \quad \forall A \in D^\theta \tag{9}$$

$$Pls(A) = \sum_{B\in D^\theta, B\cap A\neq\varnothing} m(B), \quad \forall A \in D^\theta \tag{10}$$

$$BetP(A) = \sum_{\theta_i\in A} BetP(\theta_i), \quad \forall A \in D^\theta \tag{11}$$

where

$$BetP(\theta_i) = \sum_{A\in D^\theta, \theta_i\in A} \frac{m(A)}{|A|}, \quad \forall \theta_i \in \Theta \quad i = 1,\cdots,n \tag{12}$$

$|A|$ is the cardinal of the set A

Moreover, the interval $\left[Bel(A), Pls(A)\right]$, known as the confidence interval, which quantifies the ignorance of the source on the hypothesis A, can be used for a decision.

Following this presentation of the DSmT, the material used in this study is presented in the next section.

3. Materials

The tools used are software and data.

With regard to the software, it was first used ENVI 4.7 to preprocessing ASTER images, then MATLAB to develop a model based on the use of the spectral indices NDVI, MNDWI and NDBa, and the DSmT to characterize states of the vegetation, aquatic and mineral surfaces. The data are of two types: field data and remote sensing data.

Field data consist of geographical coordinates of fixed points and outcrops. They are collected in the Toumodi-Yamoussoukro-Tiébissou area in the V Baoulé in Côte d'Ivoire. The remote sensing data used are derived from the ASTER sensor and are rectified satellite images of the scene AST_L1A_00301102004105832, covering this area. This sensor has 14 bands with a broad spectral region covering the visible and near infrared (VNIR-Visible and Near Infrared), the medium infrared (SWIR-Short-Wave Infrared: Tape 4, Band 5, Band 6, Band 7, Band 8 and Band 9) and Thermal Infrared (TIR-Thermal Infrared: Band 10, Band 11, Band 12, Band 13 and Band 14).

The spatial resolution associated with the said images is 15 m in the visible and the near infrared, 30 m in the medium infrared and 90 m in the thermal infrared.

4. Methods

The approach used consisted first of a preprocessing on the ASTER satellite images under ENVI, and then it was developed a classification model based on the calculation of spectral indices (NDVI, *MNDWI* and *NDBaI*) and the use of DSmT. Concretely, it was a question of modeling the discernment and reasoning frameworks, the mass functions as well as the functions of measuring the evidence, and defining the decision criteria. In addition, algorithms and programming codes in language were realized under Matlab software and the classified image was generated and evaluated.

4.1. Preprocessing

In order to benefit from the totality and the quality of the spatial resolutions and the spectral resolutions, the said ASTER satellite images have been subject to georeferencing, geometric correction and resampling to create a compatible database, from the 14 bands.

First, georeferencing was performed for each band using the k-nearest neigh-

bors method; then the geometric correction was made from 100 bitter points, chosen covering uniformly the ASTER scene of interest, with the bilinear method; finally, the sampling, at a step of 15 m with the bilinear method, is carried out for the SWIR (bands 4, 5, 6, 7, 8 and 9) and TIR (bands 10, 11, 12, 13 and 14) bands.

Georeferencing and geometric correction make it possible to make these satellite images superimposable on others georeferenced supports in the same coordinate system.

4.2. Development of the Model

4.2.1. Modeling of Discernment and Reasoning Frameworks

Any portion of the Earth's surface can be a combination of three main entities: a vegetation surface, an aquatic surface and a mineral surface.

In this study, a vegetation area is an area of natural and/or cultural plants; an aquatic surface is a zone of natural and/or artificial watercourses and/or water bodies; a mineral surface is an area covered by soil, rock outcrops and/or built-up. Thus, depending on the size of the area of any surface observed, it is possible to physically observe a vegetation surface, an aquatic surface, a mineral surface, a vegetation and aquatic surface, a vegetation and mineral surface, a mineral and aquatic surface or a vegetation, aquatic and mineral surface. The smaller the surface portion, the less it will contain different entities. So, an area of 15 m × 15 m could discriminate, at best on a satellite image according to the spectral characteristics, vegetation surfaces, aquatic surfaces and mineral surfaces.

Therefore, the adopted discernment framework Θ is (Equation (13)):

$$\Theta = \{E, V, M\} \tag{13}$$

where

E: aquatic surface

V: vegetation surface

M: mineral surface

By setting $\theta_1 = E$, $\theta_2 = V$, $\theta_3 = M$ and $A \cup B = \{A, B\} \quad \forall A, B \in D^{\Theta}$, the following reasoning framework ([1]) is obtained:

$$\begin{aligned} D^{\Theta} = \{&\phi, E, V, M, \{E,V\}, \{V,M\}, \{E,M\}, \Theta, E \cap V, V \cap M, E \cap M, \\ &E \cap \{V,M\}, M \cap \{E,V\}, V \cap \{E,M\}, \{V, E \cap M\}, \{M, E \cap V\}, \\ &\{E, V \cap M\}, \{E \cap M, E \cap V, V \cap M\}, E \cap V \cap M\} \end{aligned}$$

4.2.2. Modeling Information Sources

The sources of information considered in this study are the images produced by the neocanals obtained from the calculation of the spectral indices *NDVI*, *MNDWI* and *NDBaI*. These sources have been chosen because of their simplicity of calculation, their standardized character and their reputation for less sensitivity (compared to reflectances) with respect to external factors such as the geometry of the illumination or the atmospheric effects. The calculation of the spec-

tral indices *NDVI*, *MNDWI* and *NDBaI* is obtained respectively by Equations (14)-(16):

$$NDVI = \frac{\rho(bande\,3) - \rho(bande\,2)}{\rho(bande\,3) + \rho(bande\,2)} \tag{14}$$

$$MNDWI = \frac{\rho(bande\,1) - \rho(bande\,7)}{\rho(bande\,1) + \rho(bande\,7)} \tag{15}$$

$$NDBaI = \frac{\rho(bande\,14) - \rho(bande\,7)}{\rho(bande\,14) + \rho(bande\,7)} \tag{16}$$

where

$\rho(bande\,1)$: reflectance in the green (visible);
$\rho(bande\,2)$: reflectance in the red (visible);
$\rho(bande\,3)$: reflectance in the near infrared;
$\rho(bande\,7)$: reflectance in the mean infrared;
$\rho(bande\,14)$: reflectance in thermal infrared.

The values of these indices are theoretically between −1 and +1. For *NDVI*, negative values correspond to surfaces such as snow, water or clouds, for which the reflectance in the red is greater than that of the near infrared. For bare soils, with reflectance values roughly the same in red and near infrared, the *NDVI* has values close to 0. Vegetation formations have positive *NDVI* values, generally between 0.1 and 0.7. The highest values correspond to the densest vegetation cover. The *MNDWI* clearly distinguishes water surfaces (clear colors: positive values) from non-water surfaces (vegetation, castings, bare soil) (dark colors: negative values) giving more details than the *NDWI* ([15]). As for *NDBaI*, it discriminates the mineral surfaces (light colors: positive values) of the other components (dark colors: negative values) ([16]).

For a successful work, a detection of segmentation thresholds was carried out by learning for each source by reviewing those obtained by the said authors. Thus, the thresholds used and retained are recorded in the **Table 1**.

4.2.3. Modeling and Estimation of Masse Functions

The mass functions of the sources are defined on the reasoning framework D^{Θ}

$$\begin{aligned} D^{\Theta} = \{&\phi, E, V, M, \{E,V\}, \{V,M\}, \{E,M\}, \Theta, E \cap V, V \cap M, E \cap M,\\ &E \cap \{V,M\}, M \cap \{E,V\}, V \cap \{E,M\}, \{V, E \cap M\}, \{M, E \cap V\},\\ &\{E, V \cap M\}, \{E \cap M, E \cap V, V \cap M\}, E \cap V \cap M\} \end{aligned}$$

Considering the normal distribution of variable x and parameters μA and σA, in Equation (17):

Table 1. Segmentation thresholds considered for *NDVI*, *MNDWI* and *NDBaI*.

	$NDVI = X$			$MNDWI = Y$		$NDBaI = Z$	
Threshold	$X \le -0.9$	$-0.9 < X \le 0.1$	$0.1 < X$	$Y \le 0.9$	$0.9 < Y$	$Z < -0.1$	$-0.1 \le Z$
Entity	E	M	V	$\{M,V\}$	E	$\{E,V\}$	M

$$N\left(x,\mu_A,\sigma_A\right)=\frac{1}{\sigma_A\sqrt{2\pi}}\exp\left(-\frac{\left(x-\mu_A\right)^2}{2{\sigma_A}^2}\right) \tag{17}$$

with μ_A et σ_A respectively the mean and the standard deviation of the data x belonging to A, the mass functions of the sources are then defined by Equations (18)-(24).

- ***NDVI Function Mass***

With $NDVI\left(x\right)$: value of the pixel x of the $NDVI$ image, we have:

if $NDVI\left(x\right)\le -0.9$ then:

$$\begin{cases} NDVI_x\left(E\right)=\sigma_E\sqrt{2\pi}N\left(NDVI\left(x,\mu_E,\sigma_E\right)\right) \\ NDVI_x\left(\Theta\right)=1-NDVI_x\left(E\right) \\ NDVI_x\left(A\right)=0 \quad \forall A\in D^\theta-\left\{E,\Theta\right\} \end{cases} \tag{18}$$

if $-0.9\prec NDVI\left(x\right)\le 0.1$ then:

$$\begin{cases} NDVI_x\left(M\right)=\sigma_M\sqrt{2\pi}N\left(NDVI\left(x\right),\mu_M,\sigma_M\right) \\ NDVI_x\left(\Theta\right)=1-NDVI_x\left(M\right) \\ NDVI_x\left(A\right)=0 \quad \forall A\in D^\theta-\left\{M,\Theta\right\} \end{cases} \tag{19}$$

if $NDVI\left(x\right)\succ 0.1$ then:

$$\begin{cases} NDVI_x\left(V\right)=\sigma_V\sqrt{2\pi}N\left(NDVI\left(x\right),\mu_V,\sigma_V\right) \\ NDVI_x\left(\Theta\right)=1-NDVI_x\left(V\right) \\ NDVI_x\left(A\right)=0 \quad \forall A\in D^\theta-\left\{V,\Theta\right\} \end{cases} \tag{20}$$

- ***MNDWI Function Mass***

With $MNDWI\left(x\right)$: value of the pixel $\boldsymbol{x}$ of the $MNDWI$ image, we have:

if $MNDWI\left(x\right)\le 0.9$ then:

$$\begin{cases} MNDWI_x\left(\left\{M,V\right\}\right)=\sigma_{\{M,V\}}\sqrt{2\pi}N\left(MNDWI\left(x\right),\mu_{\{M,V\}},\sigma_{\{M,V\}}\right) \\ MNDWI_x\left(\Theta\right)=1-MNDWI_x\left(\left\{M,V\right\}\right) \\ MNDWI_x\left(A\right)=0 \quad \forall A\in D^\theta-\left\{\left\{M,V\right\},\Theta\right\} \end{cases} \tag{21}$$

if $MNDWI\left(x\right)\succ 0.9$ then:

$$\begin{cases} MNDWI_x\left(E\right)=\sigma_E\sqrt{2\pi}N\left(MNDWI\left(x\right),\mu_E,\sigma_E\right) \\ MNDWI_x\left(\Theta\right)=1-MNDWI_x\left(E\right) \\ MNDWI_x\left(A\right)=0 \quad \forall A\in D^\theta-\left\{E,\Theta\right\} \end{cases} \tag{22}$$

- ***NDBaI Function Mass***

With $NDBaI\left(x\right)$: value of the pixel $\boldsymbol{x}$ of the $NDBaI$ image, we have:

if $NDBaI\left(x\right)\prec -0.1$ then:

$$\begin{cases} NDBaI_x\left(\left\{E,V\right\}\right)=\sigma_{\{E,V\}}\sqrt{2\pi}N\left(NDBaI\left(x\right),\mu_{\{E,V\}},\sigma_{\{E,V\}}\right) \\ NDBaI_x\left(\Theta\right)=1-NDBaI_x\left(\left\{E,V\right\}\right) \\ NDBaI_x\left(A\right)=0 \quad \forall A\in D^\theta-\left\{\left\{E,V\right\},\Theta\right\} \end{cases} \tag{23}$$

if $NDBaI(x) \geq -0.1$ then:

$$\begin{cases} NDBaI_x(M) = \sigma_M \sqrt{2\pi} N\left(NDBaI(x), \mu_M, \sigma_M\right) \\ NDBaI_x(\Theta) = 1 - NDBaI_x(M) \\ NDBaI_x(A) = 0 \quad \forall A \in D^\theta - \{M, \Theta\} \end{cases} \tag{24}$$

Focal elements of the sources $S_1 = NDVI$, $S_2 = MNDWI$ and $S_3 = NDBaI$ are reported in Table 2.

- ***Combined Mass Function***

The combined mass function is obtained by a hybrid combination method of DSmT based on the PCR5 rule (algorithm (*Dj*)), as a function of the twelve situations generated by the thresholding conditions of $S_1(x)$, $S_2(x)$ and $S_3(x)$.

It was used on the elements of D^Θ and integrity constraint that generates four models that can reflect the reality on the ground:

- **model 1:** integrity constraint: $E \cap V \cap M = \phi$;
- **model 2:** integrity constraint: $E \cap V \cap M = \phi$ and cancellation of masses of $E \cap \{V, M\}$, $M \cap \{E, V\}$ and $V \cap \{E, M\}$;
- **model 3:** integrity constraint: $E \cap V \cap M = \phi$ and cancellation of masses of $E \cap \{V, M\}$, $M \cap \{E, V\}$, $V \cap \{E, M\}$, $\{E, V\}$, $\{V, M\}$ and $\{E, M\}$;
- **model 4:** integrity constraint: $E \cap V \cap M = \phi$ and cancellation of masses of $E \cap \{V, M\}$, $M \cap \{E, V\}$, $V \cap \{E, M\}$, $\{E, V\}$, $\{V, M\}$, $\{E, M\}$, $E \cap V = \phi$, $V \cap M = \phi$ and $E \cap M = \phi$;

Thus, for each of the twelve situations, the combined mass function is generated in the planes P_1, P_2 and P_3 ($P_1P_2P_3$), starting from the triplet of intersections formed by the focal elements of the sources S_1, S_2 and S_3, where:

Table 2. Focal elements of the sources S_1, S_2 and S_3 according to the thresholding conditions on $S_1(x)$, $S_2(x)$ et $S_3(x)$.

Situation N°	Conditions			Focal elements		
	$S_1(x) = X_1$	$S_2(x) = X_2$	$S_3(x) = X_3$	S_1	S_2	S_3
1	$X_1 \leq -0.9$	$X_2 > 0.9$	$X_3 \geq -0.1$	{*E*,Θ}	{*E*,Θ}	{*M*,Θ}
2	$X_1 \leq -0.9$	$X_2 > 0.9$	$X_3 < -0.1$	{*E*,Θ}	{*E*,Θ}	{{*E*, *V*},Θ}
3	$X_1 \leq -0.9$	$X_2 \leq 0.9$	$X_3 \geq -0.1$	{*E*,Θ}	{{*M*, *V*},Θ}	{*M*, Θ}
4	$X_1 \leq -0.9$	$X_2 \leq 0.9$	$X_3 < -0.1$	{*E*,Θ}	{{*M*, *V*},Θ}	{{*E*, *V*},Θ}
5	$X_1 > 0.1$	$X_2 > 0.9$	$X_3 \geq -0.1$	{ *V*,Θ}	{*E*,Θ}	{*M*,Θ}
6	$X_1 > 0.1$	$X_2 > 0.9$	$X_3 < -0.1$	{ *V*,Θ}	{*E*,Θ}	{{*E*, *V*},Θ}
7	$X_1 > 0.1$	$X_2 \leq 0.9$	$X_3 \geq -0.1$	{ *V*,Θ}	{{*M*, *V*},Θ}	{*M*, Θ}
8	$X_1 > 0.1$	$X_2 \leq 0.9$	$X_3 < -0.1$	{ *V*,Θ}	{{*M*, *V*},Θ}	{{*E*, *V*},Θ}
9	$-0.9 < X_1 \leq 0.1$	$X_2 > 0.9$	$X_3 \geq -0.1$	{*M*,Θ}	{*E*,Θ}	{*M*,Θ}
10	$-0.9 < X_1 \leq 0.1$	$X_2 > 0.9$	X_3 , -0.1	{*M*,Θ}	{*E*,Θ}	{{*E*, *V*},Θ}
11	$-0.9 < X_1 \leq 0.1$	$X_2 \leq 0.9$	$X_3 \geq -0.1$	{M,Θ}	{{M,V},Θ}	{M,Θ}
12	$-0.9 < X_1 \leq 0.1$	$X_2 \leq 0.9$	$X_3 < -0.1$	{M,Θ}	{{M,V},Θ}	{{E,V},Θ}

$$\begin{cases} P_1 = \{E, V, M, \Theta\} = \{1; 2; 3; 4\} \\ P_2 = \{E, \{M, V\}, \Theta\} = \{1; 2; 3\} \\ P_3 = \{M, \{E, V\}, \Theta\} = \{1; 2; 3\} \end{cases}$$

In the planes $P_1P_2P_3$, the first component of the intersection belongs to the plane P_1 and is indicated by its position in the same plane. The second and third components obey the same principle respectively in the planes P_2 and P_3.

4.2.4. Decision and Evaluation

Once all the combined mass functions of the single and multiple assumptions of a pixel x are determined, the decision rule used is the combined mass function maximum given the presence of intersections of elements in the model of DSmT ([1]).

The evaluation for this study is based first on statistical analysis and then on a visual conformance analysis. The statistical analysis is carried out by a confusion matrix $M_{CF}(k)$ based on the ground truth classes and those of the combined image by model k (k = 1, 2, 3, 4). True field classes are placed in columns while those in the combined image are in rows. The total number of pixels per class for the ground truth is distributed to the classes of the combined image. The performance indices are then calculated from Equations (25)-(28) ([2] [17]):

$$GCR_i = \frac{M_{cf}(i,i)}{N_i}, i = 1, 2, 3 \tag{25}$$

$$GCR_{moy} = \frac{\sum_{i=1}^{3} GCR_i}{3} \tag{26}$$

$$ECR_{ji} = \frac{M_{cf}(j,i)}{N_i}, \; j \neq i \tag{27}$$

$$ECR_i = \sum_{j, j \neq i} \frac{M_{cf}(j,i)}{N_i} \tag{28}$$

with ***i***: class number of truth field,

j: class number of the combined image by model,

N_i: number of pixels of class i of the ground truth,

$M_{cf}(j,i)$: number of pixels of the class i of the ground truth having been assigned after classification to the class j of the combined image by model,

GCR_i: rate of well classified pixels of class i of ground truth,

GCR_{moy}: average rate of well classified pixels of truth ground,

ECR_{ji}: rate of misclassified pixels of class i of ground truth in class j of the combined image by model,

ECR_i: rate of misclassified pixels of class i of the ground truth.

Finally, a synthetic confusion matrix M_{CF} is produced by combining the four models.

The ground truth was realized from a field reconnaissance to highlight the enti-

ties water "*E*", vegetation "*V*" and mineral "*M*". Once these entities are found, from their geographical coordinates, they are identified on the images and then sampled using the pixels.

The visual conformance analysis, on the other hand, consisted of verifying on the ground the correspondences of the various composite classes provided by the classification. Portions of the image have been chosen and their geographical coordinates determined, with which a field check is carried out.

The methodological approach used is summarized in Figure 1.

The different results obtained during this process are presented in the following section.

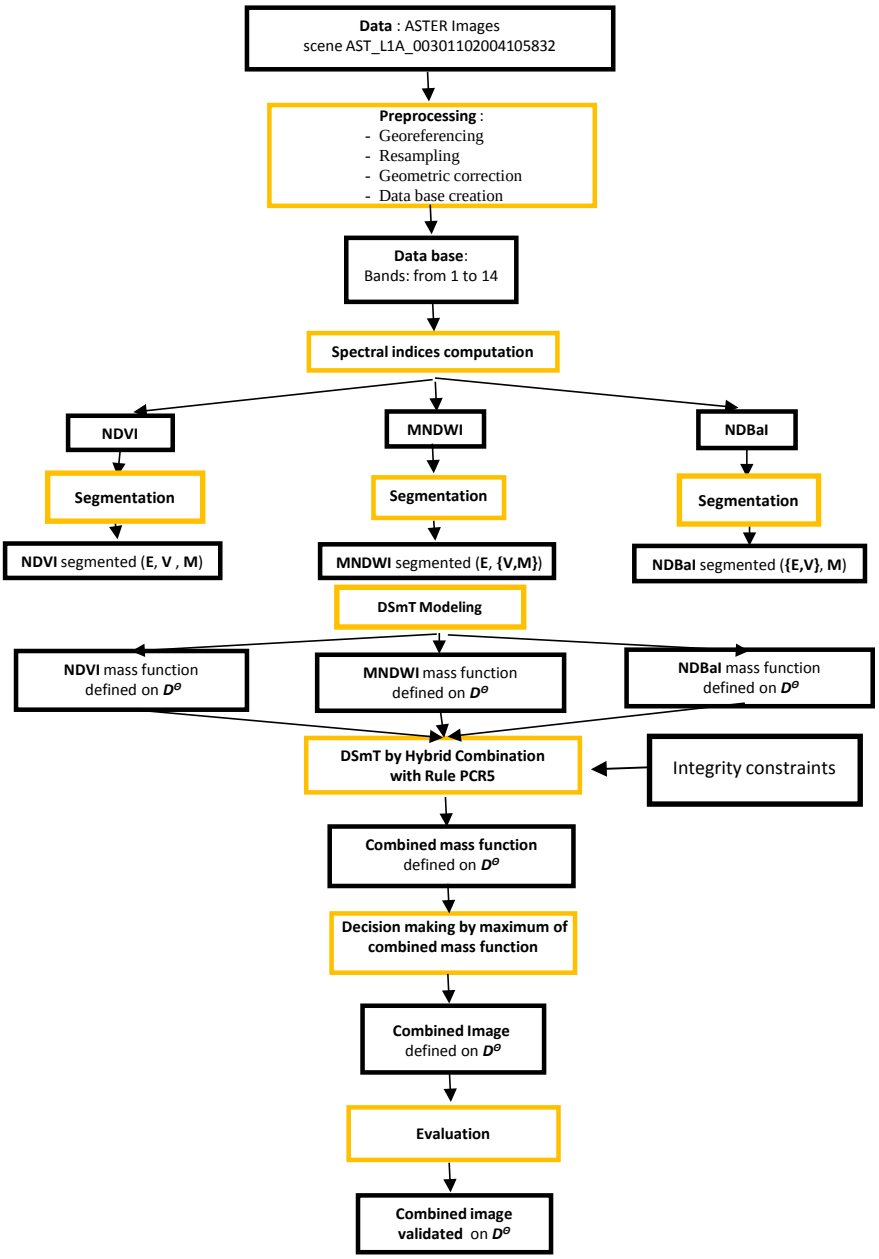

Figure 1. The flow chart of the methodology used.

5. Results and Discussions

The results presented derive from the classifications made with the hybrid DSmT based on the PCR5 rule for the above four models generated by an integrity constraint and simplifications.

5.1. Classification Models

Under the constraint of exclusion integrity $E \cap V \cap M = \phi$ for the model 1 and neglecting the masses of $E \cap \{V,M\}$, $M \cap \{E,V\}$, $V \cap \{E,M\}$, $\{E,V\}$, $\{V,M\}$, $\{E,M\}$, $E \cap V$, $M \cap V$ and $E \cap M$ in accordance with models 2, 3 and 4, Figures 2-5 respectively show the results of the classification of models 1, 2, 3 and 4 whose number of classes produced according to said models is 11, 8, 6 and 3. From a qualitative point of view, according to the model, we observe three simple classes for certain knowledge (*E*, *V*, *M*) and/or eight composite classes. The latter are formed by two classes of union characterizing partial ignorances ($\{E,V\}$, $\{M,V\}$) and six intersection classes including three simple intersection classes ($E \cap V$, $M \cap V$, $E \cap M$) and three classes of composite intersection ($E \cap \{M,V\}$, $M \cap \{E,V\}$, $V \cap \{E,M\}$), which represent paradoxes. The distribution of pixels for quantitative analysis in these different classes of images classified according to models 1, 2, 3 and 4 is recorded in Table 3. In modeling, model 1 was retained with 84.98% for single classes versus 15.02% for composite classes.

5.2. Evaluation

The evaluation was done successively from models 4, 3, 2 and 1. The statistical analysis is presented in Table 4. From model 4, well classified pixel rates for **E** (96.02%), **V** (91.51%) and **M** (99.60%) are obtained, giving an average rate of 95.74%. The pixels **E** of the ground truth are coincident with the classification pixels **V** and **M** respectively 0.29% and 3.69%, whereas the pixels **V** and **M** of the ground truth are mutually coincident with 8.41 % and 0.40%. For models 1, 2 and 3, in addition to the statistical analysis, which gives a minimal percentage of

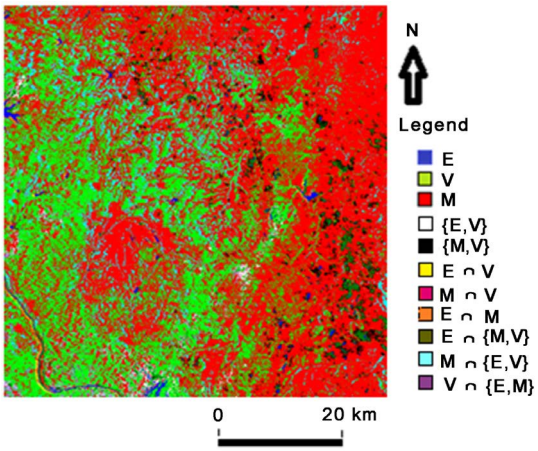

Figure 2. Image classified according to model 1.

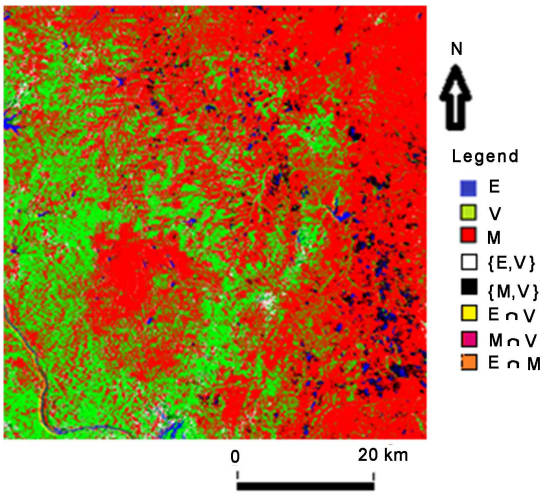

Figure 3. Image classified according to model 2.

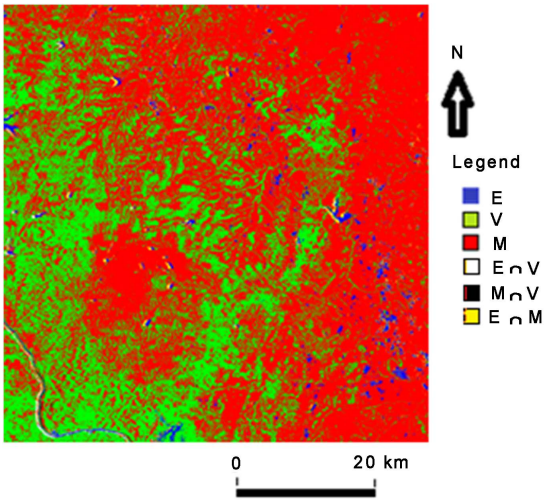

Figure 4. Image classified according to model 3.

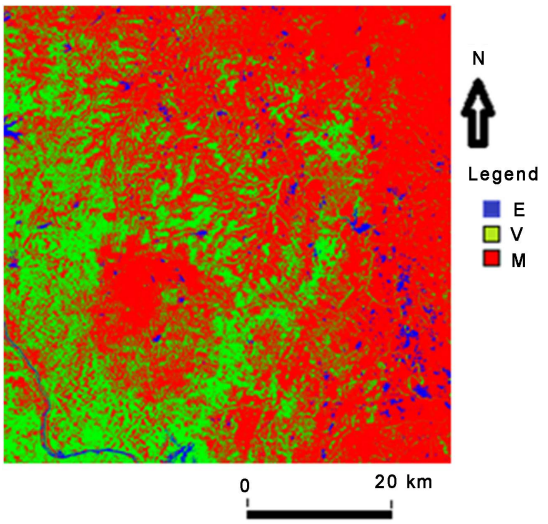

Figure 5. Image classified according to model 4.

Table 3. Distribution of pixels by class according to models 1, 2, 3 and 4.

		Model 1		Model 2		Model 3		Model 4	
		Number of pixels	% pixels	Number of pixels	% pixels	Number of pixels	% pixels	Number of pixels	% pixels
Combined and classified image	E	129,600	0.75	226,870	1.32	289,447	1.68	369,509	2.15
	V	4,767,345	27.68	4,967,525	28.85	5,250,117	30.49	5,288,132	30.71
	M	9,737,965	56.55	10,562,346	61.34	11,439,968	66.43	11,562,359	67.14
	$\{E,V\}$	208,329	1.21	566,710	3.29	0	0	0	0
	$\{M,V\}$	553,069	3.21	771,473	4.48	0	0	0	0
	$\{E,M\}$	0	0	0	0	0	0	0	0
	$E \cap V$	29,967	0.17	29,967	0.17	29,967	0.17	0	0
	$\square M \cap V$	1714	0.01	1714	0.01	75,627	0.44	0	0
	$E \cap M$	68,047	0.40	93,395	0.54	134,874	0.78	0	0
	$E \cap \{M,V\}$	218,685	1.27	0	0	0	0	0	0
	$M \cap \{E,V\}$	1,092,685	6.35	0	0	0	0	0	0
	$V \cap \{M,E\}$	412,594	2.40	0	0	0	0	0	0
TOTAL		**17,220,000**	**100**	**17,220,000**	**100**	**17,220,000**	**100**	**17,220,000**	**100**

Table 4. Synthesis confusion matrix M_{CF} combining the four models.

		Truth on the ground											
		Model 1			Model 2			Model 3			Model 4		
		E	V	M	E	V	M	E	V	M	E	V	M
Combined and classified image	E	**94.24**	0.00	0.00	**94.30**	0.00	0.00	**94.44**	0.00	0.00	**96.02**	0.00	0.00
	V	0.00	**90.67**	0.00	0.00	**91.19**	0.00	0.00	**91.27**	0.00	**0.29**	**91.59**	**0.40**
	M	0.00	**0.11**	**95.11**	0.00	**0.17**	**95.63**	**0.23**	**6.41**	**99.58**	**3.69**	**8.41**	**99.60**
	$\{E,V\}$	0.00	**3.14**	0.00	0.00	**3.14**	**1.25**	0.00	0.00	0.00	0.00	0.00	0.00
	$\{M,V\}$	0.00	**4.14**	0.00	0.00	**4.49**	**0.02**	0.00	0.00	0.00	0.00	0.00	0.00
	$\{E,M\}$	**0.62**	0.00	**0.04**	**0.70**	0.00	**0.16**	0.00	0.00	0.00	0.00	0.00	0.00
	$E \cap V$	0.00	**0.91**	0.00	**0.04**	**0.91**	0.00	0.00	**0.99**	0.00	0.00	0.00	0.00
	$\square M \cap V$	0.00	0.00	**1.97**	0.00	**0.09**	**1.97**	0.00	**1.32**	**0.42**	0.00	0.00	0.00
	$E \cap M$	**4.79**	0.00	**0.96**	**4.95**	0.00	**0.96**	**5.33**	0.00	0.00	0.00	0.00	0.00
	$E \cap \{M,V\}$	**0.35**	0.00	0.00	0.00	0.00	0.00	0.00	0.00	0.00	0.00	0.00	0.00
	$M \cap \{E,V\}$	0.00	0.00	**1.92**	0.00	0.00	0.00	0.00	0.00	0.00	0.00	0.00	0.00
	$V \cap \{M,E\}$	0.00	**1.02**	0.00	0.00	0.00	0.00	0.00	0.00	0.00	0.00	0.00	000
ECR_i		**5.76**	**9.33**	**4.89**	**5.70**	**8.81**	**4.37**	**5.56**	**8.73**	**0.42**	**3.98**	**8.41**	**0.40**

well classified pixels of 90.67%, the conformity analysis carried out in the field gives 96.37%, 94.19% and 91.02%, an average rate of 93.86%. Therefore, the initial model 1 is chosen as a model adapted to this situation.

6. Conclusion

In this article, in order to map the surface state of the Toumodi-Yamoussoukro-Tiébissou zone in the "V Baoule" of Côte d'Ivoire, the theory of plausible and paradoxical reasoning of Dézert-Smarandache was proposed with the aim of taking into account the paradoxical nature of the intersections of the vegetation surface, the aquatic surface and the mineral surface from Aster satellite images and the *NDVI*, *MNDWI* and *NDBaI* spectral indices. After a preprocessing on the ASTER satellite images, a model of surface state characterization based on the calculation of spectral indices (*NDVI*, *MNDWI* and *NDBaI*) and the DSmT with the computation PCR5 rule, was developed. It gives an average rate of 93.34% for well classified pixels and a field compliance rate of 96.37%. However, the results could be improved by a supervised approach to mass functions, in particular through the extensive use of learning elements. This model could be used, with appropriate adjustments, for other mapping purposes.

References

[1] Abbas, N. (2009) Développement de modèles de fusion et de classification contextuelle d'images satellitaires par la théorie de l'évidence et la théorie du raisonnement plausible et paradoxal. [Development of Fusion Models and Contextual Classification of Satellite Images by the theory of Evidence and the Theory of Plausible and Paradoxical Reasoning.] Thesis of Magister in Signal and Image Processing, USTHB, Alger, 76 p.

[2] Okaingni, J.-C., Kouamé, K.F. and Martin, A. (2010) Mapping Breastplates in Volcano-Sedimentary Area of Anikro-kadiokro (Ivory Coast) Using the Dempster-Shafer Theory of Evidence. *Revue Télédétection*, **9**, 19-32.

[3] Youanta, M., Kouamé, K.F., Koudou, A., Adja, M.G., Baka, D., Lasm, T., De Lasme, O., Jourda, J.P. and Biémi, J. (2014) Apport de la Cartographie Lithostructurale par Imagerie Satellitaire Landsat 7 à la Connaissance des Aquifères du Socle Précambrien de la Région de Bondoukou (Nord-Est de la Côte D'ivoire). [Contribution of Lithostructural Mapping by Landsat 7 Satellite Imagery to the Knowledge of the Aquifers of the Precambrian Base of the Bondoukou Region (Northeast of Côte d'Ivoire).] *International Journal of Innovation and Applied Studies*, **7**, 892-910.

[4] Okaingni, J.-C., Ouattara, S., Kouassi, A.F., Koné, A., Vangah, W.J. and Clement, A. (2017) Application of the Dempster-Shafer Theory to the Classification of Pixels from Aster Satellite Images and Spectral Indices. *Journal of Applied Mathematics and Physics*, **5**, 1462-1477. https://doi.org/10.4236/jamp.2017.57120

[5] Chen, X.L., Zhao, H.M., Li, P.X. and Yin, Z.Y. (2006) Remote Sensing Image Based on Analysis of the Relationship between Urban Heat Island and Land Use/Cover Changes. *Remote Sensing of Environment*, **104**, 133-146. https://doi.org/10.1016/j.rse.2005.11.016

[6] Uddin, S., Al Ghadban, A.N., Al Dousari, A., Al Murad, M. and Al Shamroukh, D. (2010) A Remote Sensing Classification for Land-Cover Changes and Micro-Climate in Kuwait. *International Journal of Sustainable Development and Planning*, **5**, 367-377. https://doi.org/10.2495/SDP-V5-N4-367-377

[7] Smarandache, F. and Dezert, J. (2004) Advances and Application of DSmT for In-

formation Fusion. American Research Press, Champaign, IL, 418 p.

[8] Dezert, J. and Smarandache, F. (2003) Partial Ordering of Hyper-Powersets and Matrix Representation of Belief Functions within DSmT. *Proceedings of 6th International Conference on Information Fusion*, Cairns, 8-11 July 2003, 1230-1238. https://doi.org/10.1109/ICIF.2003.177378

[9] Dedekind, R. (1897) Über Zerlegungen von Zahlen durch ihre grössten gemeinsammen Teiler. In: May, K., Ed., *Gesammelte Werke Bd.*1, Mohr Siebeck, Heidelberg, 103-148.

[10] Lefèvre, E. (2012) Fonctions de croyance: de la théorie à la pratique. Habilitation à diriger des recherches en genie informatique et Automatique. Ecole Doctorale Sciences pour l'Ingenieur. [Functions of Belief: From Theory to Practice. Authorization to Direct Re-Searches in Computer and Automated Engineering.] University of Artois, Lille-Nord of France, 151 p.

[11] Lowrance, J.D., Strat, T.M., Wesley, L.P., Garvey, T.D., Ruspini, E.H. and Wilkins, D.E. (1991) The Theory, Implementation and Practice of Evidential Reasoning. SRI Project 5701 Final Report, SRI, Palo Alto.

[12] Djiknavorian, P. (2008) Fusion d'informations dans un cadre de raisonnement de Dezert-Smarandache appliquée sur des rapports de capteurs ESM sous le STANAG 1241. [Fusion of Information in a Dezert-Smarandache Reasoning Framework Applied to ESM Sensor Reports under STANAG 1241.] Master's Thesis in Electrical Engineering, University of Laval, Québec, 235 p.

[13] Smarandache, F. and Dezert, J. (2006) Advances and Applications of DSmT for Information Fusion. American Research Press, Vol. 2, 442 p.

[14] Florea, M.C., Dézert, J., Valin, P., Smarandache, F. and Jousselme, A.-L. (2006) Adaptive Combination Rule and Proportional Conflict Redistribution Rule for Information Fusion. *COGIS* 2006 *Conference*, Paris, March 2006. http://www.see.asso.fr/cogis2006/pages/programme.htm

[15] Xu, H.Q. (2006) Modification of Normalized Difference Water Index (MNDWI) to Enhance Open Water Features in Remotely Sensed Imagery. *International Journal of Remote Sensing*, **27**, 3025-3033. https://doi.org/10.1080/01431160600589179

[16] Zhao, H.M. and Chen, X.L. (2005) Use of Normalized Difference Bareness Index in Quickly Mapping Bare Areas from TM/ETM+. *International Geoscience and Remote Sensing Symposium*, Seoul, 25-29 July 1973, Vol. 3, 1666-1668.

[17] Martin, A., Laanaya, H. and Arnold-Bos, A. (2006) Evaluation for Uncertain Image Classification and Segmentation. *Pattern Recognition*, **39**, 1987-1995.